

Topological Peierls instabilities in more than one dimension

Santiago Palumbo,¹ Pablo S. Cornaglia,^{1,2} and Jorge I. Facio^{1,2}

¹*Instituto Balseiro, Univ. Nacional de Cuyo, Av. Bustillo, 9500, Argentina*

²*Centro Atómico Bariloche, Instituto de Nanociencia y Nanotecnología (CNEA-CONICET), Av. Bustillo, 9500, Argentina*

(Dated: March 28, 2025)

A periodic lattice distortion that reduces the translational symmetry folds electron bands into a reduced Brillouin zone, leading to band mixing and a tendency to gap formation, as in the Peierls transition in one-dimensional systems. However, in higher dimensions, the resulting phase can present topological obstructions preventing a complete gap opening. We discuss two different mechanisms for such obstructions, emergent Weyl nodes and symmetry protected band crossings. Based on density-functional calculations, we show these mechanisms are at play in trigonal PtBi_2 .

Introduction. The coupling between electron and lattice degrees of freedom is often key to understanding the emergence of electronic and structural order in complex materials. A textbook example is the Peierls transition, where a one-dimensional (1D) lattice becomes unstable toward dimerization, resulting in a reduced translational symmetry and an associated charge density wave [1]. This transition leads to the opening of a gap in the electron spectrum which lowers the system's total energy, and stabilizes the distorted, insulating phase. Soon after periodic lattice distortions were observed in quasi-1D systems [2], charge density waves were discovered in effectively two-dimensional (2D) materials [3, 4]. Since then, understanding the ingredients introduced by the higher dimensionality has remained a topical question [5–9].

The fundamental connection between symmetries and topological phases in electronic systems [10–14] naturally raises the question of how electronic topology is altered when translational symmetry is reduced [15–25]. This symmetry reduction leads to band folding into a smaller Brillouin zone, resulting in band crossings. While these crossings are generally subject to level repulsion and gap openings, symmetry constraints can enforce protected band crossings at specific wave vectors. Additionally, band-touching points may naturally arise in three-dimensional systems even in the absence of explicit symmetry protections [26–28]. Weyl and Dirac points serve as prominent examples of such crossings, where topological invariants protect the degeneracies and lead to robust surface states or exotic transport phenomena [29]. These crossings can prevent a full gap from developing at the Fermi level, leading to a topologically obstructed Peierls phase, in which levels are repelled from the Fermi energy, leaving behind a pseudogap in the spectrum.

As an example of this physics, we identify trigonal PtBi_2 , a noncentrosymmetric Weyl semimetal [30–34] that has recently garnered attention for its superconducting phase [30, 31, 35–38]. Within a certain temperature range, this superconducting phase has been found to be exclusive to the topological Fermi arcs [31], underscoring the importance of a detailed understanding of the electronic structure in the normal phase.

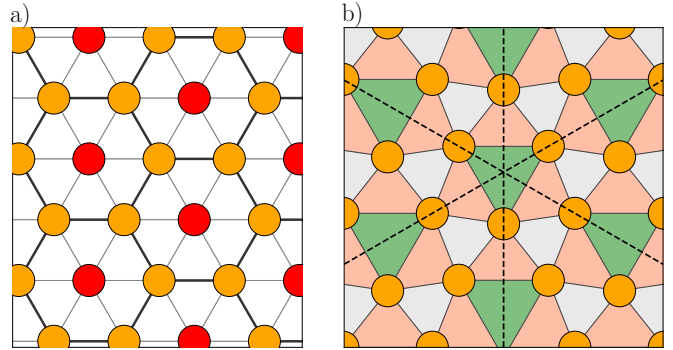


FIG. 1. Examples of distortions of the triangular lattice that reduce translational symmetry while preserving threefold rotational and reflection symmetries. (a) Atoms shown as darker shaded disks are displaced out of the plane, forming a buckled, decorated honeycomb lattice. (b) The equilateral triangles are distorted into triangles of varying sizes, creating sequences of alternating small and large side-sharing triangles along the mirror planes.

In this Letter, we address the effects of translation symmetry reduction, focusing on systems with triangular lattice symmetry and connecting in a single framework the physics of honeycomb- and Kagome-based systems. We demonstrate different ways in which the electronic reconstruction associated with this symmetry reduction can stabilize a topological semimetallic phase. Finally, based on density-functional calculations of PtBi_2 , we show that this obstructed Peierls mechanism gives origin to the nontrivial topology of its normal phase.

A 2D Peierls instability. Our starting point is a 2D triangular lattice. In Fig. 1, we present two examples of structural distortions that reduce its translational symmetry while preserving threefold rotational and reflection symmetries present in trigonal PtBi_2 . In these examples, sequences of short and long bonds can be identified, as in the 1D Peierls case, but the patterns can not be reduced to a mere stack of weakly coupled chains of dimerized bonds, underscoring their inherently 2D nature. In Fig. 1a), one out of three atoms is displaced out of the plane, resulting in a buckled, decorated honeycomb lattice. In Fig. 1b), one out of three atoms moves along a mirror-

invariant line, leading to sequences of side-sharing small and large triangles along each of such lines.

In the latter case, the resulting $\sqrt{3} \times \sqrt{3}$ supercell can be described using lattice vectors $\mathbf{a} = (3/2, -\sqrt{3}/2)$ and $\mathbf{b} = (0, \sqrt{3})$ expressed in units of the triangular lattice parameter, and sites $\mathbf{s}_1 = -\lambda \mathbf{a}/3$, $\mathbf{s}_2 = \lambda(\mathbf{a} + \mathbf{b})/3$ and $\mathbf{s}_3 = -\lambda \mathbf{b}/3$, inside the unit cell. Here, λ is a distortion parameter that interpolates between the triangular lattice ($\lambda = 1$) and the Kagome lattice ($\lambda = 1.5$). To illustrate the main effects of this distortion on the electronic structure we consider a spinless tight-binding Hamiltonian with a single s orbital on each site,

$$H(\mathbf{k}) = -tF(\mathbf{k}) + \delta D(\mathbf{k}), \quad (1)$$

where the first term on the r.h.s. describes the nearest-neighbor hoppings and the second term introduces their change due to the structural distortion [Fig. 2a)]. The nonzero elements of $F(\mathbf{k})$ read

$$\begin{aligned} F_{12}(\mathbf{k}) &= e^{i\mathbf{k}\cdot(\mathbf{s}_1-\mathbf{s}_2)} \left(1 + e^{-i\mathbf{k}\cdot\mathbf{a}} + e^{-i\mathbf{k}\cdot(\mathbf{a}+\mathbf{b})}\right), \\ F_{13}(\mathbf{k}) &= F_{12}(M_x\mathbf{k}), \\ F_{23}(\mathbf{k}) &= F_{12}(C_3^{-1}\mathbf{k}), \end{aligned} \quad (2)$$

where M_x and C_3 are, respectively, the reflection operation, which acts like $M_x : \mathbf{a} \rightarrow -\mathbf{a} - \mathbf{b}$, and the three-fold rotation $C_3 : \mathbf{a} \rightarrow \mathbf{b}$. The tensor $D(\mathbf{k})$ has the same symmetry properties and

$$D_{12}(\mathbf{k}) = e^{i\mathbf{k}\cdot(\mathbf{s}_1-\mathbf{s}_2)} \left(1 - e^{-i\mathbf{k}\cdot\mathbf{a}} - e^{-i\mathbf{k}\cdot(\mathbf{a}+\mathbf{b})}\right). \quad (3)$$

The case $\delta > 0$ describes the situation in which the hopping amplitude along shorter (longer) bonds increases (decreases). As detailed in the Supplementary Material (SM), $H(\mathbf{k})$ preserves time-reversal, three-fold rotational, and mirror symmetries across planes containing the rotation axis [39].

For $\delta = 0$, which corresponds to the triangular lattice, the system recovers inversion (I) symmetry as well as additional translations, making the use of a supercell unnecessary. In this case, the band structure can be obtained by folding the bands of the triangular lattice into the reduced Brillouin zone. Although this is no longer possible in the presence of a distortion, the band structure can nevertheless partially retain the folding pattern. This can be quantified by the so-called unfolding weight w_{nk} , which measures the overlap between a Bloch state with wave-vector k and band number n and the state with the same wave-vector on the undistorted lattice [40, 41]. For $\delta = 0$, folded and non-folded bands have weights $w_{nk} = 0$ and $w_{nk} = 1$, respectively.

As in 1D, band folding leads to band crossings at the BZ boundary, here, e.g., at the K point [Fig. 2b,c)]. However, unlike in 1D, the crossing at K involves three bands, reflecting that this point is equidistant from three adjacent BZ centers [42]. In addition, along Γ - K , the folded

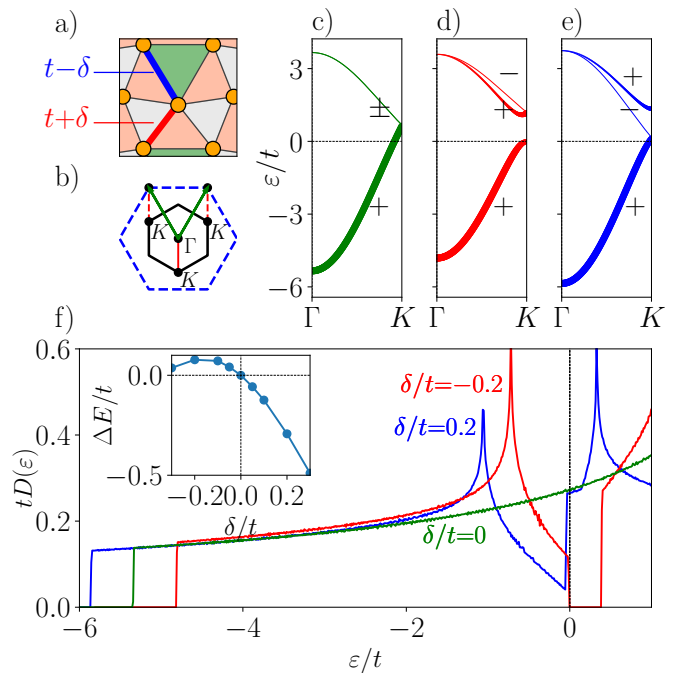


FIG. 2. (a) Fragment of the distorted lattice [see Fig. 1b)] indicating the hopping amplitudes for short ($t + \delta$) and long ($t - \delta$) bonds. (b) Brillouin zones corresponding to the triangular lattice (dashed blue lines) and to the $\sqrt{3} \times \sqrt{3}$ supercell (black continuous lines). The supercell Brillouin zone is rotated by 30° and reduced in area by a factor of three relative to the original lattice. (c) Undistorted triangular lattice band structure folded into the supercell Brillouin zone. The reflection symmetry eigenvalues are indicated by + and - signs next to the bands. The linewidth indicates the unfolding weight which is 1 for the lower band and 0 for the upper bands in this case. The Fermi level ($\epsilon_F = 0$) corresponds to an occupancy of a single electron per unit cell. (d,e) Band structure for the distorted case with (d) $\delta/t = -0.2$ and (e) $\delta/t = 0.2$. (f) Density of states for $\delta/t = 0.2, 0$, and 0.2 . Inset: Total electronic energy relative to the undistorted limit as a function of δ/t .

bands are doubly degenerate due to the reflection symmetry, which pairs reciprocal lattice vectors, causing bands in the associated BZs to fold to the same energy along this path in the supercell first BZ.

Folding induced degeneracies are lifted once the translation symmetry is reduced. In particular, the three-fold crossing at K is split, although not necessarily generating a full gap opening. That is the case for $\delta < 0$, as shown in Fig. 2d), where both the double degeneracy of the folded bands along Γ - K and their crossing at K with the non-folded bands gap out. Conversely, for $\delta > 0$, a Dirac cone carrying a non-trivial Berry phase emerges at K [Fig. 2e)].

These two scenarios can be classified by the mirror-symmetry eigenvalues of the Bloch states. The little group of both Γ and K contains C_3 and reflection symmetries, allowing the formation of two-dimensional irreducible representations with states of opposite mirror

eigenvalues. The two folded bands at Γ form such a representation and have two possible ways of connecting with the states at K : they split in energy and pair again at K , or they swap, with one folded band crossing at K with the non-folded band.

Thus, the sign of δ controls a phase transition between an insulator and a symmetry-enforced topological semimetal. Notably, the latter phase can be smoothly connected with Kagome-like systems, with a flat band and a Dirac cone at K obtained in the present model in the $\delta \rightarrow t$ limit. Similar obstructions to a full gap opening can be obtained for the distortion in Fig. 1a). An important difference in this case is that the point symmetry of the atomic sites includes C_3 . For this reason, the distorted electronic structure is smoothly connected to the honeycomb lattice case. Other possible distortions of the triangular lattice and the effects of longer range hoppings are analyzed in the SM [39].

Fig. 2f) illustrates that a finite δ has a significant effect on the electronic structure near the Fermi level and on the total bandwidth. Since the short bonds form continuous pathways across the system, when $\delta > 0$ their increased hopping amplitude leads to an increased bandwidth. Conversely, as the long bonds form large triangles connected to each other only through short bonds [see Fig. 1b)], $\delta < 0$ favors charge localization at these large triangles and thus a bandwidth reduction.

These changes modify the total electronic energy relative to the undistorted case (ΔE), as depicted in the inset of Fig. 2f). For both signs of δ , the strong low-energy reconstruction, from a metal at $\delta = 0$ to either an insulator for $\delta < 0$ or to a semimetal for $\delta > 0$, transfers spectral weight from the Fermi level to lower energies, reducing the total electronic energy. The bandwidth change leads to an additional reduction of the energy for $\delta > 0$ while it competes with the Fermi level effect for $\delta < 0$. For small δ this results in $\Delta E \propto \delta$, showing that the electronic contributions can drive a finite distortion.

The case of a bilayer. Let us consider a stack of two triangular lattices, based as before on a $\sqrt{3} \times \sqrt{3}$ supercell setting. In the absence of a distortion, the layers are connected by inversion symmetry. Atoms in one layer are positioned as in the previous section (shifted by a finite amount along the stacking direction), while those in the second layer obey $\mathbf{s}_{i+3} = -\mathbf{s}_i$, with $i = \{1, 2, 3\}$. We consider the Hamiltonian

$$H_b(\mathbf{k}) = \begin{pmatrix} -tF(\mathbf{k}) & \nu C(\mathbf{k}) \\ \nu C^\dagger(\mathbf{k}) & -tF(\mathbf{k}) \end{pmatrix} + \begin{pmatrix} \delta D(\mathbf{k}) & 0 \\ 0 & 0 \end{pmatrix}. \quad (4)$$

The first term on the right hand side describes the centrosymmetric limit, including in-plane first-neighbor hoppings within each layer as well as an interlayer first-neighbor coupling described by $C(\mathbf{k})$. In order to ensure the same symmetries than in the monolayer, we have $C_{ij}(\mathbf{k}) = g(C_3^{\eta_{ij}} \mathbf{k})$, where $\eta_{ij} = \epsilon_{ij}(-1)^{i+j}$, with ϵ_{ij} the 2D Levi-Civita tensor and $g(\mathbf{k}) = e^{i\mathbf{k} \cdot (\mathbf{s}_1 - \mathbf{s}_4)}$. The sec-

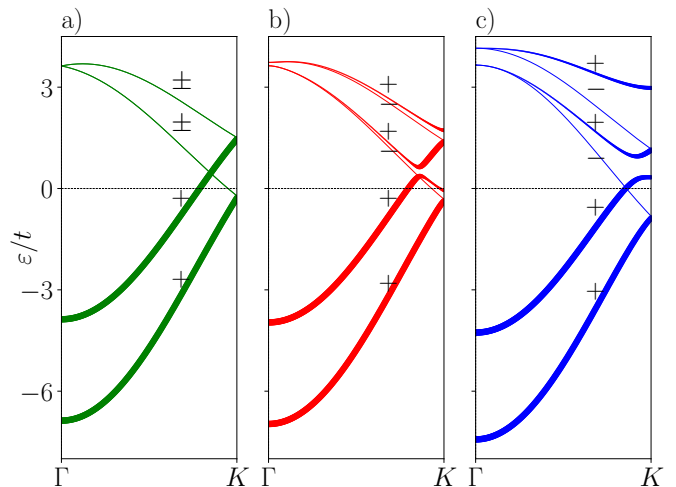


FIG. 3. Band structure of a triangular AB stacked bilayer (a) without distortion and (b,c) with one of the layers dimerized: (b) $\delta/t = 0.1$ and (c) $\delta/t = 0.5$. Energies are measured with respect to the $1/3$ filling chemical potential. As in Fig. 2, the linewidth indicates the unfolding weight and the reflection symmetry eigenvalues are indicated with + and - signs.

ond term reduces the translation symmetry by distorting only one of the layers.

For $\delta = 0$ and finite interlayer coupling ν , the band structure resembles the monolayer case, yet it is effectively doubled due to formation of bonding and antibonding states. As a result, there are two three-fold crossings at K . Typically, the folded pair of bands associated with one of these crossings at K can intersect with the non-folded band involved in the second crossing. This intersection forms a three-fold crossing that can occur at any momentum along Γ - K and is also unstable under perturbations that reduce the translational symmetry. Nonetheless, as in the monolayer, any perturbation that preserves the reflection symmetry will allow the intersection between the non-folded band and its folded counterpart of opposite mirror eigenvalue to persist, as exemplified in Fig. 3c).

Thus, the dimerization in a bilayer stabilizes a topological semimetal albeit in this case the topological band crossing is no longer pinned at the BZ border. This mechanism is also relevant in three dimensional systems where the translational symmetry is reduced along two dimensions. For a stack of coupled bilayers, which reproduces the Bi crystal structure in PtBi_2 , the above analysis can be easily extended to each k_z plane, resulting in the formation of a mirror-protected nodal line.

The case of PtBi_2 . Fig. 4a) shows the crystal structure of PtBi_2 in the space group $P31m$ (157) [43, 44]. Distorted triangular lattices as those in Fig. 1 are stacked along with a Pt triangular lattice every two Bi layers. The centrosymmetric parent phase formed by undistorted triangular lattices can be stabilized by substituting Bi with Te or Sb [45]. The distortion linking these

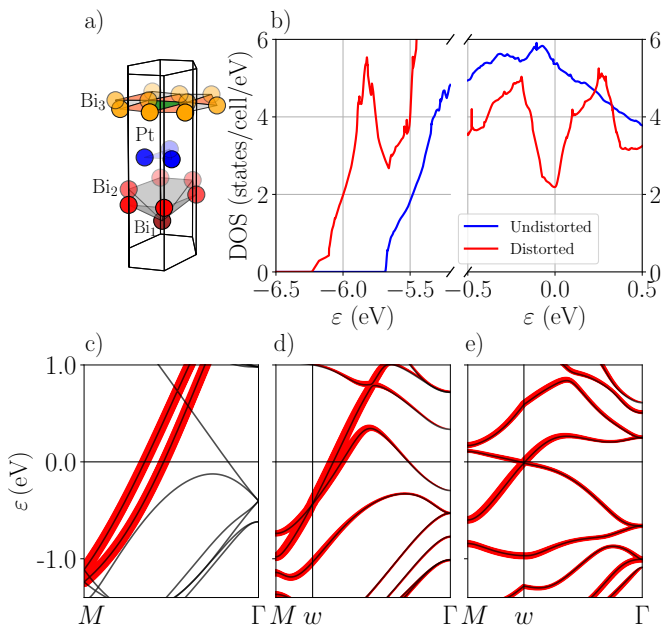


FIG. 4. (a) Crystal structure of PtBi₂. (b) Density of states in the absence of SOC for the undistorted (space group P3̄2/m1) and distorted (P31m) crystal structures. (c,d,e) Band structure of in the absence of spin-orbit coupling for different crystal structures, the size of the red dots indicates the unfolding weight: c) centrosymmetric limit ($\alpha = 0$) where the unfolding weight exactly distinguished folded bands; d) intermediate value of $\alpha = 0.39$ where Weyl nodes emerge; e) noncentrosymmetric case ($\alpha = 1$).

two structures controls a transition between a metal and a topological semimetal [46]. This strong electronic reconstruction originates in the reduction of translational symmetry and, accordingly, it is weakly affected by the SOC. We next focus on the case without SOC to demonstrate that even in its absence, the semimetallic phase is characterized by the emergence of Weyl nodes. This explicitly shows that the purely-orbital physics involved in inversion-breaking Peierls instabilities in three dimensions can stabilize a Weyl phase. A detailed discussion of the effects of SOC, along with estimates of the hopping amplitude asymmetries induced by the reduced translational symmetry, is presented in [46].

We perform *ab-initio* calculations using the experimentally reported structure of noncentrosymmetric PtBi₂ [44] (S_0) and of centrosymmetric Pt(Bi_{0.901}Te_{0.099})₂ [45] (S_1), in both cases representing the systems with the space group P31m [39]. We also consider intermediate structures obtained as $S_\alpha = (1-\alpha)S_0 + \alpha S_1$, $0 \leq \alpha \leq 1$.

Fig. 4b) shows the density of states (DOS), which reveals a pronounced reduction at the Fermi level in the noncentrosymmetric case compared to the centrosymmetric one, which is indicative of a metal-to-semimetal transition. In addition, the distorted structure leads to an approximately 0.5 eV increase in the overall bandwidth.

The band structure near the Γ point illustrates how the suppression of spectral weight takes place (Fig. 4c-e). In the undistorted case, states from the BZ border are folded to Γ at -0.4 eV. The distortion splits their degeneracy, opening a gap of 0.8 eV at this wave-vector. The resulting phase is yet not insulating due to the emergence of topological crossings. These include nodal lines within mirror-invariant planes, the origin of which follows the ideas discussed in the previous section. Secondly, and more interesting as it best illustrates key aspects linked to the dimensionality, the distortion also leads to the pairwise creation of Weyl nodes.

These nodes involve bands that at $\delta = 0$ can be identified as folded and non-folded. They are not present for arbitrarily small distortions, rather, they emerge from the Γ - M lines at a finite value of $\alpha \approx 0.39$ and persist for α up to 1. They are monopoles of the Berry curvature which, without spin-orbit coupling, has as only sources orbital and site degrees for freedom.

The dimensionality, as well as the fact that the distortion not only reduces translational symmetry but also breaks inversion symmetry, are essential. Indeed, in a time-reversal symmetric three-dimensional system, codimension arguments indicate that this symmetry breaking can drive the system into a stable Weyl phase [27]. In PtBi₂, while the Peierls distortion pushes spectral weight away from the Fermi energy, the created crossings introduce an obstruction—inextricably linked to the three-dimensional nature of the system—that prevents a full charge gap from opening. Importantly, as shown in Ref. [46], these crossings are robust to inclusion of the SOC, which essentially couples the nodes of each spin sector, leading to a splitting of the Weyl nodes in energy.

Conclusions. We have analyzed Peierls instabilities in systems with triangular lattice symmetry, where translation symmetry is reduced. As in the one-dimensional Peierls transition, the electronic reconstruction contributes to stabilizing the crystal distortion. However, the fate of the electronic structure is constrained by a topological obstruction that prevents the opening of a full gap. We have examined cases where this obstruction arises from a band crossing that carries a Berry phase of π , as well as cases involving a Chern number of 1. Our findings establish a smooth connection with the limiting cases of both Kagome and honeycomb lattices and suggest that materials based on distorted triangular lattices may host the electronic instability we describe. As an illustrative example, we have argued that the topology of trigonal PtBi₂ can be effectively understood within this framework.

Acknowledgments. JF acknowledges useful discussions with Riccardo Vocaturo, Klaus Koepf, Oleg Janson, Ion Cosma Fulga, and Jeroen van den Brink.

- [1] R. E. Peierls, *Quantum Theory of Solids* (Oxford : Clarendon Press, 1955), URL <https://doi.org/10.1093/acprof:oso/9780198507819.001.0001>.
- [2] R. Comès, M. Lambert, H. Launois, and H. R. Zeller, *Phys. Rev. B* **8**, 571 (1973), URL <https://link.aps.org/doi/10.1103/PhysRevB.8.571>.
- [3] J. A. Wilson, F. J. Di Salvo, and S. Mahajan, *Phys. Rev. Lett.* **32**, 882 (1974), URL <https://link.aps.org/doi/10.1103/PhysRevLett.32.882>.
- [4] J. Wilson, F. D. Salvo, and S. Mahajan, *Adv. Phys.* **24**, 117 (1975), URL <https://doi.org/10.1080/00018737500101391>.
- [5] M.-H. Whangbo, E. Canadell, P. Foury, and J.-P. Pouget, *Science* **252**, 96 (1991), URL <https://www.science.org/doi/abs/10.1126/science.252.5002.96>.
- [6] M. D. Johannes and I. I. Mazin, *Phys. Rev. B* **77**, 165135 (2008), URL <https://link.aps.org/doi/10.1103/PhysRevB.77.165135>.
- [7] J. Laverock, D. Newby, E. Abreu, R. Averitt, K. E. Smith, R. P. Singh, G. Balakrishnan, J. Adell, and T. Balasubramanian, *Phys. Rev. B* **88**, 035108 (2013), URL <https://link.aps.org/doi/10.1103/PhysRevB.88.035108>.
- [8] K. Rossnagel, *J. Condens. Matter Phys.* **23**, 213001 (2011), URL <https://iopscience.iop.org/article/10.1088/0953-8984/23/21/213001/pdf>.
- [9] J.-P. Pouget and E. Canadell, *Rep. Prog. Phys.* **87**, 026501 (2024), URL <https://dx.doi.org/10.1088/1361-6633/ad124f>.
- [10] A. Kitaev, in *AIP Conf. Proc.* (American Institute of Physics, 2009), vol. 1134, pp. 22–30, URL <https://pubs.aip.org/aip/acp/article-abstract/1134/1/22/815164/Periodic-table-for-topological-insulators-and>.
- [11] S. Ryu, A. P. Schnyder, A. Furusaki, and A. W. Ludwig, *New J. Phys.* **12**, 065010 (2010), URL <https://doi.org/10.1088/2F1367-2630%2F12%2F6%2F065010>.
- [12] B. Bradlyn, L. Elcoro, J. Cano, M. G. Vergniory, Z. Wang, C. Felser, M. I. Aroyo, and B. A. Bernevig, *Nature* **547**, 298 (2017), URL <https://www.nature.com/articles/nature23268>.
- [13] H. C. Po, A. Vishwanath, and H. Watanabe, *Nat. Commun.* **8**, 50 (2017).
- [14] J. Kruthoff, J. de Boer, J. van Wezel, C. L. Kane, and R.-J. Slager, *Phys. Rev. X* **7**, 041069 (2017), URL <https://link.aps.org/doi/10.1103/PhysRevX.7.041069>.
- [15] C.-X. Liu, X.-L. Qi, and S.-C. Zhang, *Phys. E: Low-Dimens. Syst. Nanostructure* **44**, 906 (2012), ISSN 1386-9477, sI:Topological Insulators, URL <https://www.sciencedirect.com/science/article/pii/S1386947711004000>.
- [16] Z. Wang and S.-C. Zhang, *Phys. Rev. B* **87**, 161107 (2013), URL <https://link.aps.org/doi/10.1103/PhysRevB.87.161107>.
- [17] H. Wei, S.-P. Chao, and V. Aji, *Phys. Rev. Lett.* **109**, 196403 (2012), URL <https://link.aps.org/doi/10.1103/PhysRevLett.109.196403>.
- [18] B. Roy and J. D. Sau, *Phys. Rev. B* **92**, 125141 (2015), URL <https://link.aps.org/doi/10.1103/PhysRevB.92.125141>.
- [19] J. Gooth, B. Bradlyn, S. Honnali, C. Schindler, N. Kumar, J. Noky, Y. Qi, C. Shekhar, Y. Sun, Z. Wang, et al., *Nature* **575**, 315 (2019), URL <https://www.nature.com/articles/s41586-019-1630-4>.
- [20] B. J. Wieder, K.-S. Lin, and B. Bradlyn, *Phys. Rev. Res.* **2**, 042010 (2020), URL <https://link.aps.org/doi/10.1103/PhysRevResearch.2.042010>.
- [21] X. Zhang, Q. Gu, H. Sun, T. Luo, Y. Liu, Y. Chen, Z. Shao, Z. Zhang, S. Li, Y. Sun, et al., *Phys. Rev. B* **102**, 035125 (2020), URL <https://link.aps.org/doi/10.1103/PhysRevB.102.035125>.
- [22] Y. Li, Z. Wu, J. Zhou, K. Bu, C. Xu, L. Qiao, M. Li, H. Bai, J. Ma, Q. Tao, et al., *Phys. Rev. B* **102**, 224503 (2020), URL <https://link.aps.org/doi/10.1103/PhysRevB.102.224503>.
- [23] J. Yu, B. J. Wieder, and C.-X. Liu, *Phys. Rev. B* **104**, 174406 (2021), URL <https://link.aps.org/doi/10.1103/PhysRevB.104.174406>.
- [24] P. Li, B. Lv, Y. Fang, W. Guo, Z. Wu, Y. Wu, D. Shen, Y. Nie, L. Petaccia, C. Cao, et al., *Sci. China: Phys. Mech. Astron.* **64**, 237412 (2021).
- [25] G. Giovannetti, M. Capone, J. van den Brink, and C. Ortix, *Phys. Rev. B* **91**, 121417 (2015), URL <https://link.aps.org/doi/10.1103/PhysRevB.91.121417>.
- [26] M. V. Berry, *Aspects of Degeneracy* (Springer US, Boston, MA, 1985), pp. 123–140, ISBN 978-1-4613-2443-0, URL https://doi.org/10.1007/978-1-4613-2443-0_8.
- [27] S. Murakami, *New J. Phys.* **9**, 356 (2007), URL <https://dx.doi.org/10.1088/1367-2630/9/9/356>.
- [28] D. Vanderbilt, *Berry phases in electronic structure theory: electric polarization, orbital magnetization and topological insulators* (Cambridge University Press, 2018).
- [29] N. P. Armitage, E. J. Mele, and A. Vishwanath, *Rev. Mod. Phys.* **90**, 015001 (2018), URL <https://link.aps.org/doi/10.1103/RevModPhys.90.015001>.
- [30] A. Veyrat, V. Labracherie, D. L. Bashlakov, F. Caglieris, J. I. Facio, G. Shipunov, T. Charvin, R. Acharya, Y. Naidyuk, R. Giraud, et al., *Nano Lett.* **23**, 1229 (2023), URL <https://doi.org/10.1021/acs.nanolett.2c04297>.
- [31] A. Kuibarov, O. Suvorov, R. Vocaturo, A. Fedorov, R. Lou, L. Merkwitz, V. Voroshnin, J. I. Facio, K. Koepernik, A. Yaresko, et al., *Nature* **626**, 294–299 (2024), ISSN 1476-4687, URL <http://dx.doi.org/10.1038/s41586-023-06977-7>.
- [32] S. Hoffmann, S. Schimmel, R. Vocaturo, J. Puig, G. Shipunov, O. Janson, S. Aswartham, D. Baumann, B. Büchner, J. v. d. Brink, et al., *Adv. Phys. Res.* p. 2400150 (2024), URL <https://onlinelibrary.wiley.com/doi/full/10.1002/apxr.202400150>.
- [33] R. Vocaturo, K. Koepernik, J. I. Facio, C. Timm, I. C. Fulga, O. Janson, and J. van den Brink, *Phys. Rev. B* **110**, 054504 (2024), URL <https://link.aps.org/doi/10.1103/PhysRevB.110.054504>.
- [34] E. O’Leary, Z. Li, L.-L. Wang, B. Schruck, A. Eaton, P. C. Canfield, and A. Kaminski, arXiv:2503.08841 (2025), URL <https://arxiv.org/abs/2503.08841>.
- [35] D. L. Bashlakov, O. E. Kvitnitskaya, G. Shipunov, S. Aswartham, O. D. Feyta, D. V. Efremov, B. Büchner, and Y. G. Naidyuk, *Low Temp. Phys.* **48**, 747 (2022), URL <https://doi.org/10.1063/10.0014014>.
- [36] S. Schimmel, Y. Fasano, S. Hoffmann, J. Besproswanny, L. T. Corredor Bohorquez, J. Puig, B.-C. Elshalem, B. Kalisky, G. Shipunov, D. Baumann, et al., *Nat. Com-*

- mun. **15**, 9895 (2024), URL <https://www.nature.com/articles/s41467-024-54389-6>.
- [37] J. Zabala, V. F. Correa, F. J. Castro, and P. Pedrazzini, *J. Phys. Condens. Matter* **36**, 285701 (2024), URL <https://dx.doi.org/10.1088/1361-648X/ad3878>.
- [38] X. Di, H. Ji, W. Gao, M. Tian, H. Wang, and J. Wang, *Quantum Frontiers* **3**, 18 (2024), URL <https://link.springer.com/article/10.1007/s44214-024-00065-1>.
- [39] See the Supplementary Material, which includes a reference to [47] for (i) an analysis of other crystalline distortions realizing symmetry-obstructed Peierls instabilities, (ii) a description of the symmetries of the model Hamiltonians, and (iii) methodological details regarding DFT calculations.
- [40] E. van Heumen, J. Vuorinen, K. Koepnik, F. Masee, Y. Huang, M. Shi, J. Klei, J. Goedkoop, M. Lindroos, J. van den Brink, et al., *Phys. Rev. Lett.* **106**, 027002 (2011), URL <https://link.aps.org/doi/10.1103/PhysRevLett.106.027002>.
- [41] W. Ku, T. Berlijn, and C.-C. Lee, *Phys. Rev. Lett.* **104**, 216401 (2010), URL <https://link.aps.org/doi/10.1103/PhysRevLett.104.216401>.
- [42] Y. W. Li, J. Jiang, H. F. Yang, D. Prabhakaran, Z. K. Liu, L. X. Yang, and Y. L. Chen, *Phys. Rev. B* **97**, 115118 (2018), URL <https://link.aps.org/doi/10.1103/PhysRevB.97.115118>.
- [43] M. Kaiser, A. I. Baranov, and M. Ruck, *Z. Anorg. Allgem. Chem.* **640**, 2742–2746 (2014).
- [44] G. Shipunov, I. Kovalchuk, B. R. Piening, V. Labracherie, A. Veyrat, D. Wolf, A. Lubk, S. Subakti, R. Giraud, J. Dufouleur, et al., *Phys. Rev. Mater.* **4**, 124202 (2020), URL <https://link.aps.org/doi/10.1103/PhysRevMaterials.4.124202>.
- [45] K. Takaki, M. Yamamoto, M. Nakajima, T. Takeuchi, H. Y. Nguyen, M. Nohara, Y. Kishioji, T. Fujii, K. Yoshino, S. Miyasaka, et al., *J. Phys. Soc. Jpn* **91**, 034703 (2022), ISSN 1347-4073, URL <http://dx.doi.org/10.7566/JPSJ.91.034703>.
- [46] S. Palumbo, P. Cornaglia, and J. Facio (2025), to be submitted.
- [47] D. Malterre, B. Kierren, Y. Fagot-Revurat, C. Didiot, F. G. De Abajo, F. Schiller, J. Cerdón, and J. Ortega, *New J. Phys.* **13**, 013026 (2011), URL <https://iopscience.iop.org/article/10.1088/1367-2630/13/1/013026>.